

# Size effect of compressed concrete in four point bending RC beams

A.P. Fantilli & P.Vallini

*Politecnico di Torino, Torino, Italy*

I. Iori

*University of Parma, Parma, Italy*

**ABSTRACT:** A numerical model is proposed to study the mechanical behaviour and ductility of reinforced concrete beams in bending. We focus on the experimental results of Weiss, Güler and Shah (2001), where a size effect on the average strain of compressed concrete has been measured by changing the distance of external loads in four point bending beams. In order to reproduce numerically these results, in the proposed approach the mechanical response of RC beams, and their ductility, are calculated by modelling the progressive crushing of compressed concrete. In particular, a previous model has been extended to reproduce the effects due to different boundary conditions in the tested beams. A good agreement between numerical and experimental results has been obtained in the beams with high and low reinforcement ratio, both in the case of high strength concrete (HSC) and normal strength concrete (NSC).

**Keywords:** four point bending RC beams, compressed concrete, ductility, size effect.

## 1 INTRODUCTION

The mechanical behaviour of compressed concrete has recently been the object of several investigations (Markeset & Hillerborg 1995; Bazant & Xiang 1997; Wang & Shrive 1995). The numerical and experimental models carried out in this field have mainly regarded the post peak softening branch of the stress-strain relationship. Generally, in this stage, progressive damage produces an increase of compressive strains and a decrease of stresses. All these phenomena can affect the measure of ductility, whose magnitude shows a size effect.

In the paper of Weiss et al. (2001) for example, the flexural behaviour of reinforced concrete beams with different constant-moment zone lengths is investigated. In particular, for each length, the mean value of compressive strains is evaluated. Since the damage is localised in different zones of constant moment, the beams show different ductility, despite the same cross section.

The theoretical evaluation of “size effect” has generally been significant in structural analysis since the time of Leonardo da Vinci or Galileo Galilei, when an increase of material strength with the decrease of structural dimensions was observed. Thus, in order to obtain a quantitative analysis of the

mechanisms involved in the response of reinforced concrete beams in bending, a theoretical model is proposed. We focus on the ultimate stage before failure of reinforced concrete (RC) beams and, in particular, on the evaluation of structural ductility and its size effect.

The model proposed in this paper refers to the tests of Weiss et al. (2001), regarding four groups of beams, having different concrete strength (high HSC or normal NSC) and different percentages of reinforcement (high HR or low LR). Each group contains four beams with the same cross-section but different constant-moment zone length  $L$  (respectively 1, 2, 3, and 4 times the effective depth  $d$  of the cross section). Figure 1a shows the tested beam, whereas the main mechanical properties of materials and the percentage of steel reinforcement are summarised in Table 1. Results indicate that damage occurs in the compressed concrete of constant-moment zone, whose average moment curvature relationships  $M-\mu$  (Fig. 1b) consequently show softening branches of different slopes. A decrease in ductility with the increase of  $L$  is evident.

Therefore, it seems necessary to investigate the failure stage of reinforced concrete beams by modelling the damage mechanisms localised in the compressed concrete.

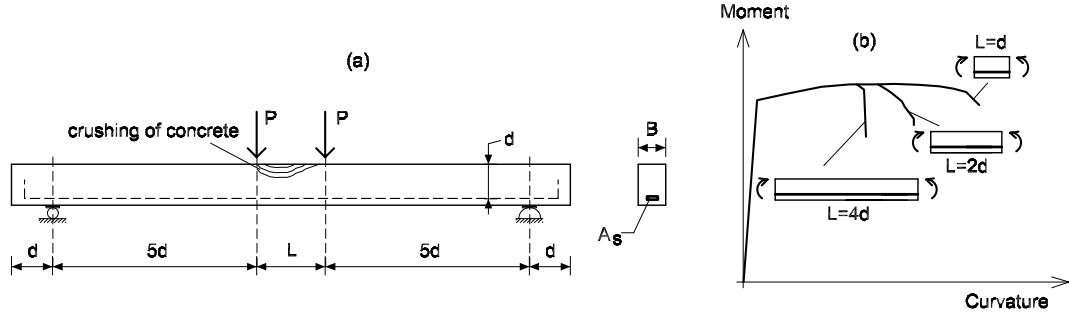


Figure 1. The beams tested by Weiss et al. (2001): a) static conditions; b) moment curvature responses.

Table 1. Mechanical and geometrical properties of the beams tested by Weiss et al. (2001).

Beams	$f_c$ MPa	$A_s$ mm <sup>2</sup>	$f_y$ MPa	$f_u$ MPa
NSC-LR-1d	39.8	138.8	395	557
NSC-LR-2d	46.6	138.8	395	557
NSC-LR-3d	46.6	138.8	395	557
NSC-LR-4d	39.8	138.8	395	557
NSC-HR-1d	38.7	382.3	400	634
NSC-HR-2d	38.7	382.3	400	634
NSC-HR-3d	46.7	382.3	400	634
NSC-HR-4d	46.7	382.3	400	634
HSC-LR-1d	98.8	382.3	400	634
HSC-LR-2d	100.6	382.3	400	634
HSC-LR-3d	100.6	382.3	400	634
HSC-LR-4d	98.8	382.3	400	634
HSC-HR-1d	108.3	981.8	431	614
HSC-HR-2d	97.9	981.8	431	614
HSC-HR-3d	97.9	981.8	431	614
HSC-HR-4d	108.3	981.8	431	614

## 2 FORMULATION OF A THEORETICAL MODEL

The mechanical response of concrete prisms subjected to uniaxial compression (Fig. 2a) can be divided into two stages (Fig. 2b). In the first stage, when the stress is lower than the concrete strength  $f_c$ , the material can be considered undamaged. As soon as the peak stress is reached, localised damage develops in the element and the second stage begins. In this stage, the progressive sliding of two blocks of concrete (Fig. 2a) and the softening branch (Fig. 2b) are evident. In Figure 2a, the angle  $\alpha$  between the horizontal face of the prism and the sliding surface is assumed to be  $17.5^\circ$ , according to the experimen-

tal observations of Fujita et al. (1998). In the cases of uniaxial compression, similar values of  $\alpha$  are obtained through the Mohr-Coulomb failure criterion, if the tensile strength of concrete  $f_{ct}$  is assumed to be  $1/10$  of the compressive one.

Both elastic shortening of the undamaged concrete and displacement between the two blocks along the sliding surface (where crack is localised) rule the average post-peak compressive strain  $\epsilon_c$  of the prism (Fig. 2). According to some experimental results, the slope of softening branch of Fig. 2b increases in longer concrete prisms because of the relationship  $w/H$  involved in the evaluation of  $\epsilon_c$ . Therefore, longer prisms behave in a more brittle manner, and sometimes snap-back can appear in the stress-strain relationship. In particular, referring to the symbols depicted in Fig. 2, post peak strains and stresses can be respectively defined by the following equations:

$$\epsilon_c = \epsilon_c^* + \frac{w}{H} = \epsilon_{c1} + \frac{\Delta\sigma_c}{E_c} + \frac{s \cos\alpha}{H} \quad (1)$$

$$\Delta\sigma_c = -a \cdot f_c \cdot w = -a \cdot f_c \cdot s \cdot \cos\alpha \quad (2)$$

where  $a = 0.1$  is the reciprocal of the mean slope of the curve  $\sigma_c/f_c - w$  (Fujita et al. 1998). Assuming  $K = a f_c \cos\alpha$ , it is possible to obtain:

$$\Delta\sigma_c = -K \cdot s, \quad \sigma_c = f_c - K \cdot s \quad (3)$$

and substituting (3) into (1), and rearranging:

$$s = \frac{\epsilon_c - \epsilon_{c1}}{\frac{\cos\alpha}{H} - \frac{K}{E_c}} \quad (4)$$

For the beam of Figure 3a, assuming plane sections compatibility, the strain profile of a generic cross-section (Fig. 3b) can be computed through the following equation:

$$\epsilon = \mu \cdot y \quad (5)$$

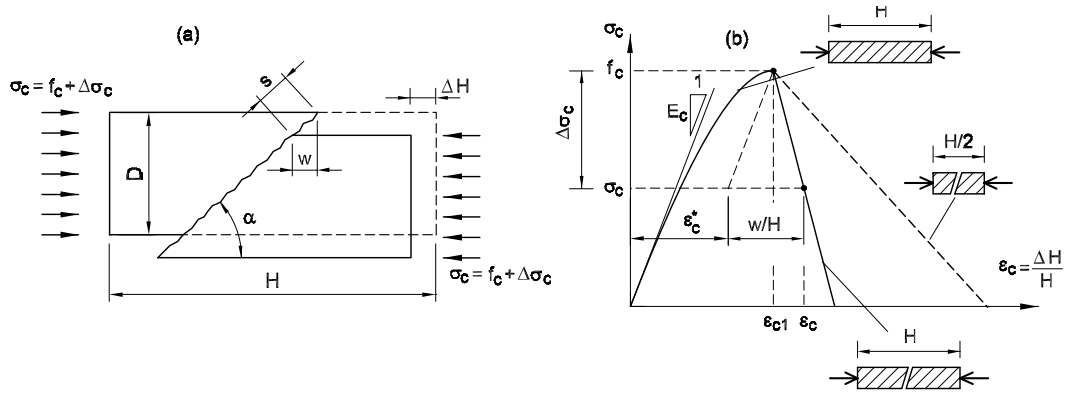


Figure 2. Damage localization in compressed concrete: the tests of Jansen & Shah (1997).

The strains that exceed  $\epsilon_{c1}$ , which rule the evolution of sliding planes, are split up into several rectangles of base  $\Delta\epsilon_{ci}$  (Figs. 3b, 3c). Due to the increase of  $\epsilon_{c,max}$ , the increments  $\Delta\epsilon_{ci}$  and the sliding planes progressively involve wider zones of the beam. However, in case of constant bending moment, it is not possible to define univocally both the evolution of the sliding planes and their slip increments  $\Delta s_i$ . For the sake of simplicity, in this paper, the number of planes originated by  $\Delta\epsilon_{ci}$  is assumed to be as low as possible. This assumption is founded on the hypothesis that new sliding planes are more probably originated by previous fracture surfaces. Therefore, only one of the possible crack pattern is depicted in Figure 3. In case of three point bending beams (Fig. 4), new sliding planes start from the cross-sections with higher bending moment, so that the crack pattern configuration is less ambiguous (Fig. 4c). In all cases, the strain increment  $\Delta\epsilon_{ci}$ , related to the displacement increment  $\Delta s_i$  (Fig. 5), affects a volume of concrete in compression with height  $y_i^*$  and length  $2H_i$ :

$$y_i^* = \frac{\epsilon_{c,max} - \epsilon_{ci}}{\mu} \quad (6)$$

$$H_i = \frac{y_i^*}{\tan \alpha} \quad (7)$$

where  $\alpha$  is the angle of the sliding planes with respect to the horizontal line (Fig. 5c).

For a given strain increment  $\Delta\epsilon_{ci}$  (Fig. 5b), the displacement variation  $\Delta s_i$ , affecting the height  $y_i^*$  (Fig. 5c), can be computed by substituting (6) and (7) into (4):

$$\begin{aligned} \Delta s_i &= \frac{\Delta\epsilon_{ci}}{\frac{\mu \cdot \sin \alpha}{\epsilon_{c,max} - \epsilon_{ci}} - \frac{K}{E_c}} = \\ &= \frac{(\epsilon_{c,max} - \epsilon_{ci}) \cdot E_c \cdot \Delta\epsilon_{ci}}{\mu \cdot \sin \alpha \cdot E_c - K \cdot (\epsilon_{c,max} - \epsilon_{ci})} \end{aligned} \quad (8)$$

The derivation of  $s_i$  with respect to  $y$  can be also evaluated from the following equation:

$$\frac{ds_i}{dy} = \frac{E_c \cdot \mu \cdot (y_{c,max} - y_{ci})}{E_c \cdot \sin \alpha - K \cdot (y_{c,max} - y_{ci})} \quad (9)$$

By means of Eq.(3), the concrete stress can also be obtained by a differential equation:

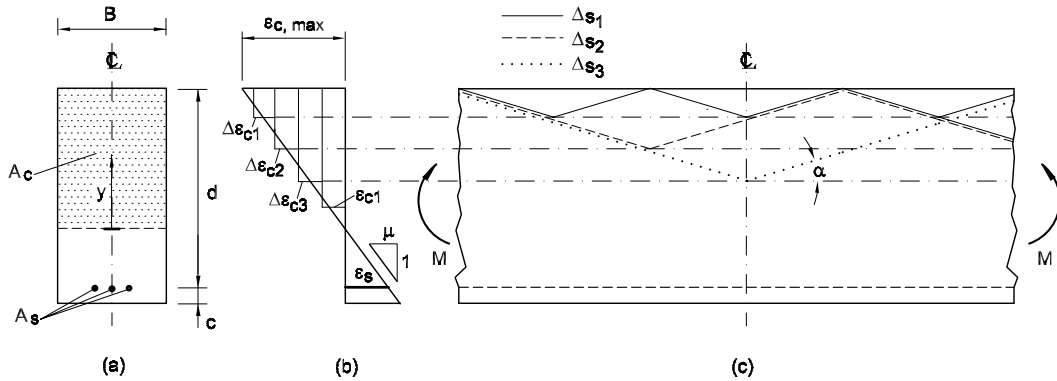


Figure 3. Reinforced concrete element in bending: a) cross-section; b) longitudinal strain profile; c) constant-moment zone.

$$d\sigma = -K \cdot \frac{ds}{dy} = \frac{K \cdot E_c \cdot \mu \cdot (y_{c,max} - y_{ci})}{E_c \cdot \sin\alpha - K \cdot (y_{c,max} - y_{ci})} \quad (10)$$

and, according to Fantilli et al. (2002a), when  $\epsilon_{c1} < \epsilon_c < \epsilon_{c,max}$ , the stress of compressed concrete can be computed with the equation:

$$\sigma_c = f_c - \frac{E_c^2 \cdot \mu \cdot \sin\alpha}{K} \quad (11)$$

$$\cdot \ln \left[ \frac{\mu \cdot E_c \cdot \sin\alpha - y_{c,max} \cdot K + K \cdot \epsilon_c}{\mu \cdot E_c \cdot \sin\alpha - y_{c,max} \cdot K + K \cdot \epsilon_{c1}} \right] + E_c \cdot (\epsilon_c - \epsilon_{c1})$$

In this equation, the stress  $\sigma_c$  depends on the extension of the compressive zone  $y_{c,max}$ , according to the size effect model of Hillerborg (1990). However, in the proposed approach, the mechanical response of compressed concrete is also a function of the cross-sectional curvature  $\mu$ . When  $\epsilon_c < \epsilon_{c1}$  the following uniaxial stress-strain relationship of CEB-FIP Model Code (1991) is adopted for the ascending branch of concrete in compression:

$$\sigma_c = \frac{\frac{E_c \cdot \epsilon_c}{E_{c1} \cdot \epsilon_{c1}} - \left(\frac{\epsilon_c}{\epsilon_{c1}}\right)^2}{1 + \left(\frac{E_c}{E_{c1}} - 2\right) \cdot \frac{\epsilon_c}{\epsilon_{c1}}} \cdot f_c \quad (12)$$

where  $E_{c1} = f_c / \epsilon_{c1}$ .

When a confinement tension  $\sigma_3$  is present (e.g. due to stirrups), the values of  $f_c$  and  $\epsilon_{c1}$ , which appear in the Equations (11) and (12), increase. By assuming the linear envelope failure of Figure 6a, the relationship between the concrete strength  $f_c$  and  $\sigma_3$  is easily evaluated as:

$$f_c = f_c^* + b \cdot \sigma_3 \quad (13)$$

where:

$$b = \frac{1 + \sin\varphi}{1 - \sin\varphi};$$

$f_c^*$  is the nominal strength without confinement stresses ( $\sigma_3 = 0$ ) and  $\varphi$  is the angle of internal friction. The increase of  $f_c$  is accompanied by an incre-

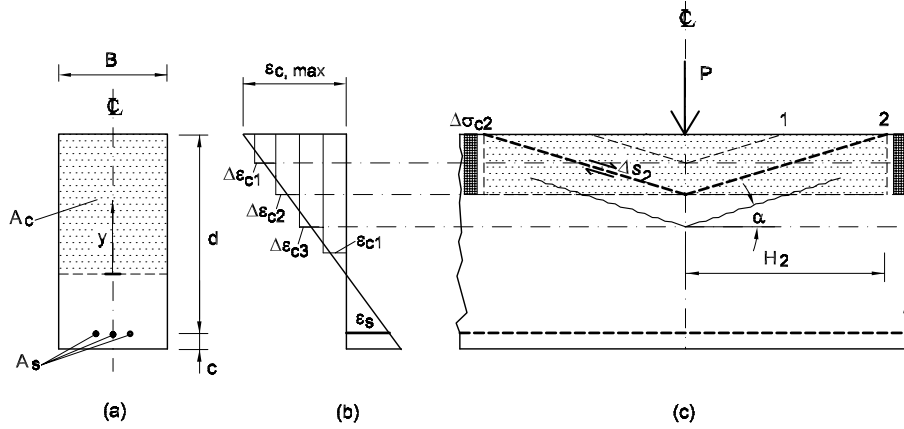


Figure 4. Reinforced concrete element in bending: a) cross-section; b) longitudinal strain profile; c) linear variation of the moment.

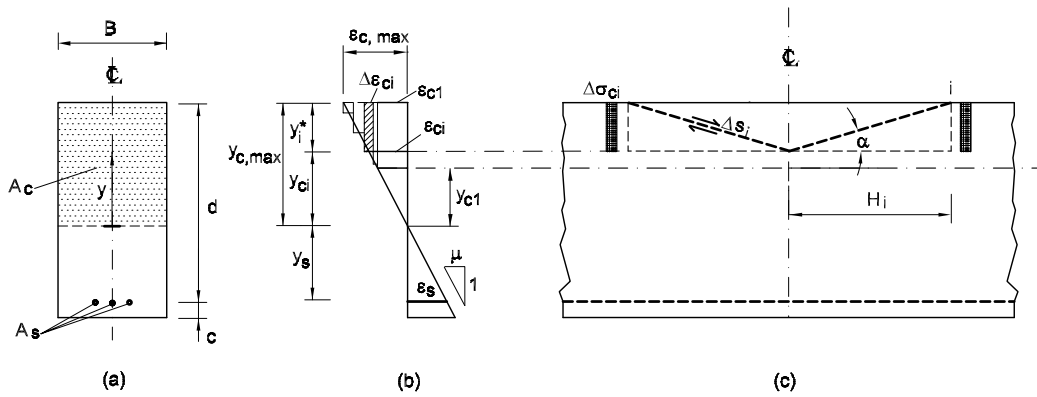


Figure 5. Reinforced concrete element in bending: a) cross-section; b) longitudinal strain profile; c) longitudinal sliding.

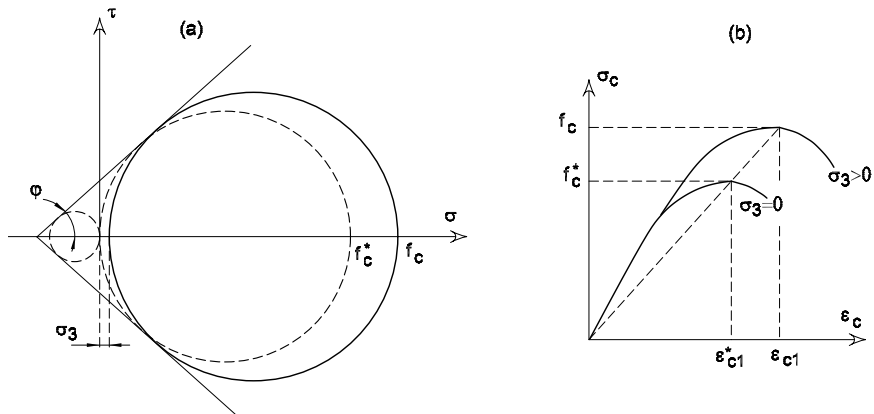


Figure 6. Confinement produced by stirrups (Fantilli et al. 2002b): a) linear envelope for concrete strength; b) increment of  $f_c$  and  $\epsilon_{c1}$ .

ment of the peak-strain  $\epsilon_{c1}$ , whose growth is assumed to be directly related to  $f_c$  (Fig. 6b):

$$\epsilon_{c1} = \epsilon_{c1}^* \frac{f_c}{f_c^*} \quad (14)$$

where  $\epsilon_{c1}^*$  and  $\epsilon_{c1}$  are respectively the peak-strains for unconfined ( $\sigma_3 = 0$ ) and for confined ( $\sigma_3 > 0$ ) concrete.

In the constant-moment zone  $L$  of a four point bending beam, the unfailing scatter of concrete strength makes the definition of crack pattern more ambiguous. Figure 7a, for example, shows a possible displacement configuration when in Section 1 a reduced strength, with respect to Section 2, has been detected. The bearing capacity of the beam (i.e. the maximum moment  $M_{u1}$ ) must be evaluated in Section 1. In the zones closer to this Section, the increase of curvature after the peak produces both a reduction of the bending moment  $M$  and an exten-

sion of damaged zone in compressed concrete. In other zones (Section 2), where the maximum moment  $M_{u2}$  has not been reached, the decrease of  $M$  produces an elastic decrease of curvature  $\mu$ . Therefore, as for the compressed concrete prisms of Figure 2, the failure mechanism is localised in a part of the beam. In particular, the softening branch of the  $M$ - $\mu$  diagram, evaluated in the constant-moment zone, shows an increasing slope with the increase of  $L$ . Such a failure is similar the failure of compressed concrete cylinders.

It must be also observed a reduced ductility of four point bending beams with larger  $L$ , because localised damage is smeared on wider zones. In other words, the post peak behaviour is ruled by the softening branch of the moment -curvature  $M$ - $\mu$  relationship of the weakest section (Section 1 in Fig. 7c), whereas, in the other zones elastic unloading should be considered (Section 2 in Fig. 7c).

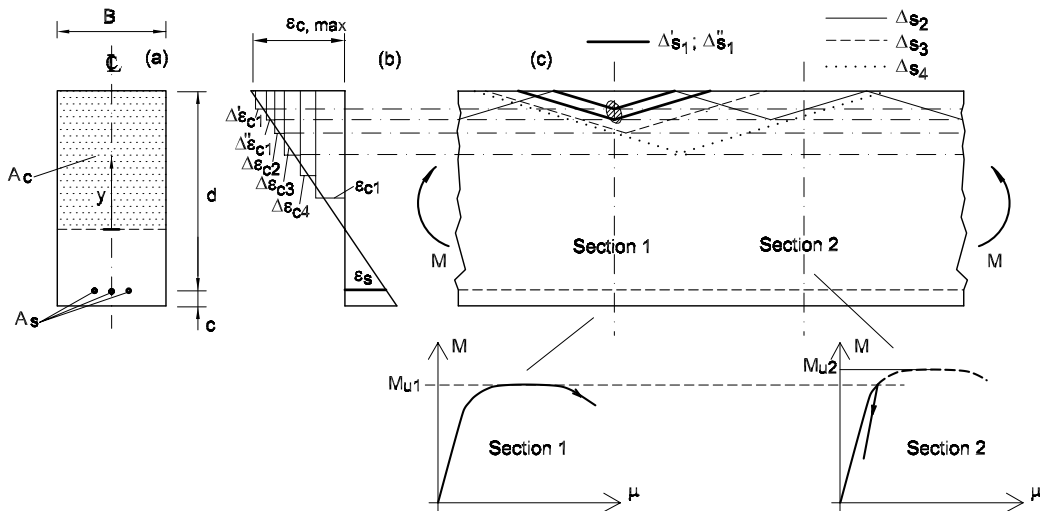


Figure 7. Reinforced concrete element in bending: a) cross-section; b) longitudinal strain profile; c) damage localization in the constant-moment zone.

Although the position of the weakest section in the constant-moment zone is always unknown, its existence cannot be neglected. In fact, due to series-connection between all the sections in these zones, only the weakest one can follow the quasi-horizontal branch that precedes the peak of the moment curvature diagrams (Fig. 7c). In this way, except for the zone with the lower strength (where the damage is localised), the other sections of the beam cannot release all their potential ductility. Starting from these assumptions, it is possible to explain the dependence of four point bending beams ductility on the constant-moment zone length, as observed in the tests by Weiss et al. (2001).

### 3 COMPARISON BETWEEN THE EXPERIMENTAL RESULTS OF WEISS ET AL. (2001) AND THE NUMERICAL RESULTS OF THE PROPOSED MODEL

The higher ductility of the beams with a shorter constant-moment zone length (Weiss et al. 2001) cannot be theoretically reproduced through Equations (11) and (12). In these equations, both damage localiza-

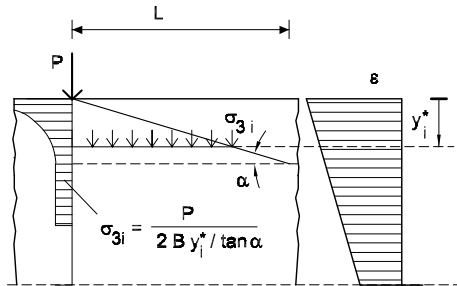


Figure 8. Confinement produced by the applied forces  $P$ .

tion and confinement produced by external load  $P$  are not taken into account. Due to  $P$ , the compressed concrete is confined and its strength shows a local increase according to Equations (13) and (14)

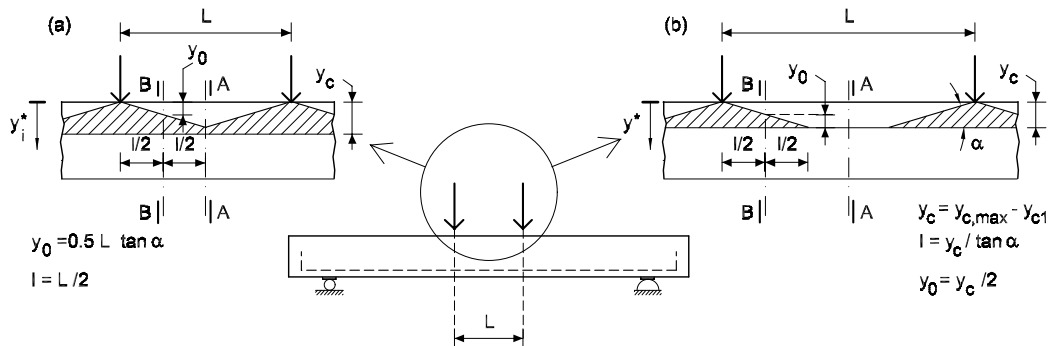


Figure 9. Confinement in the constant-moment zone: a) confinement in the whole length  $L$ ; b) confinement in a part of  $L$ .

(Fig. 8). To reproduce numerically this phenomenon, it is necessary to define the geometry of confined zones. As is shown in Figure 9, the confined zones are bounded on the top of the beam by the sliding planes of compressed concrete, which start from the points where the loads are applied. Since they extend to the border of compressed zone where the concrete strength is reached (incipient sliding), the whole constant-moment zone can be confined (Fig. 9a). This is true in the cases of short distance between the applied forces or deep compressed zones (high reinforcement ratio).

For the sake of simplicity, the mechanical response is obtained by analysing two representative sections: Section AA and Section BB of Figure 9. As is explained before, since a series connection between cross-sections is established in the constant-moment zone, damage starts in the cross-section with the lowest concrete strength. In particular, in proximity of loads  $P$ , sliding planes grow from unconfined concrete to confined zones (with a higher resistance). Schematically this behaviour is reproduced by the Section B-B of Figures 9a, 9b, where an average confinement  $\sigma_3 = P / (2 B y_i^* / \tan \alpha)$  is assumed for  $y_i^* > y_0$ . In the zones closer to Section B-B, concrete sliding displacements increase, thus their values are doubled with respect to the ones obtained from Equation (9). Section AA is located in the middle of the constant-moment zone, where confinement stresses  $\sigma_3$  are lower compared to Section BB (Fig. 9a), or null as in the case of Figure 9b.

The mean deformability of the constant-moment zone can be obtained by considering the effect of damage localization in the Section (A-A or B-B) with the lower peak moment in the  $M$ - $\mu$  relationship. Consequently, the descending post-peak branch is ruled by the softening behaviour of the damaged cross-section and by the linear elastic unloading of the undamaged ones. Both these contributes are assumed as directly proportional to referring zone length.

#### 4 CONCLUSIONS

According to the tests, a strict correlation between the ductility and constant-moment zone length  $L$  is shown by the numerical results of the proposed model. This is evident in Figure 10 and Figure 11, where the mean compressive top fiber strains  $\epsilon_{me}$  experimentally evaluated are compared with the numerical ones. A little discrepancy is revealed for beams HSC-LR, made of high strength concrete and low reinforcement ratio (Fig. 11), for which the maximum bending moment and ductility are overestimated. In the case of lower reinforced concrete beams the magnitude of damaged zones, approximately equivalent to depth of compressed concrete, can drastically reduce the ductility contribution of the undamaged cross-sections. Therefore, the peak moment is reached when the inelastic strains are lower than the ones of undamaged concrete.

To analyse the ultimate stage of reinforced concrete beams, a mechanical model for compressed concrete has been proposed by Fantilli et al. (2002a). Afterwards, this approach has been extended to confined concrete subjected to compressive loads in order to simulate the effectiveness of stirrups confinement (Fantilli et al. 2002b). In the present paper, the model has been further refined with the aim of reproducing different boundary conditions of tests. The good agreement between the numerical results and the experimental measures of Weiss et al. (2001) demonstrate the effectiveness of the model in computing the mechanisms that affect reinforced concrete beams during the ultimate stage. In particular, it is possible to define the zones where the maximum strains are localised, and consequently to evaluate the flexural response of reinforced concrete beams and its size dependence (with regard to length and height).

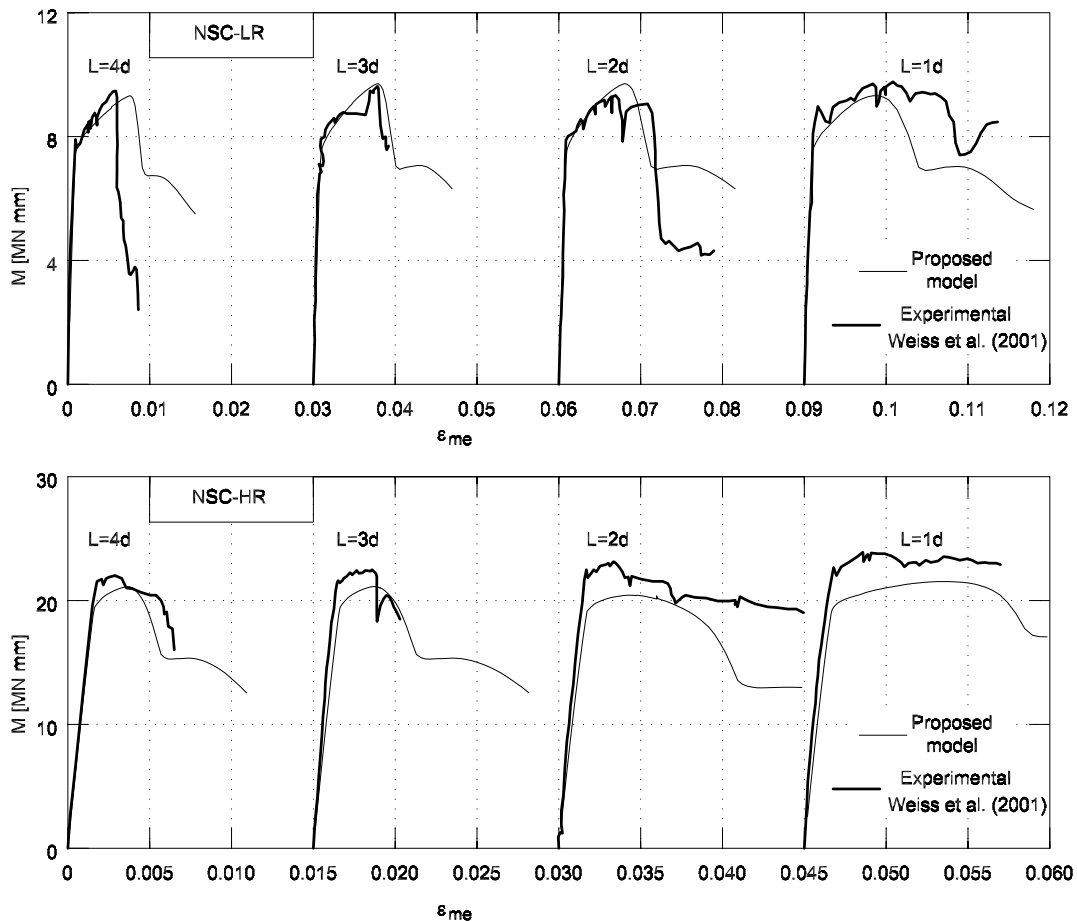


Figure 10. Average compressive top fiber strain  $\epsilon_{me}$  in the constant-moment zone  $L$ : comparison between the numerical results of the proposed model and the experimental ones by Weiss et al. (2001), measured for the beams of normal strength concrete (NSC) with high (HR) and low (LR) reinforcement ratio.

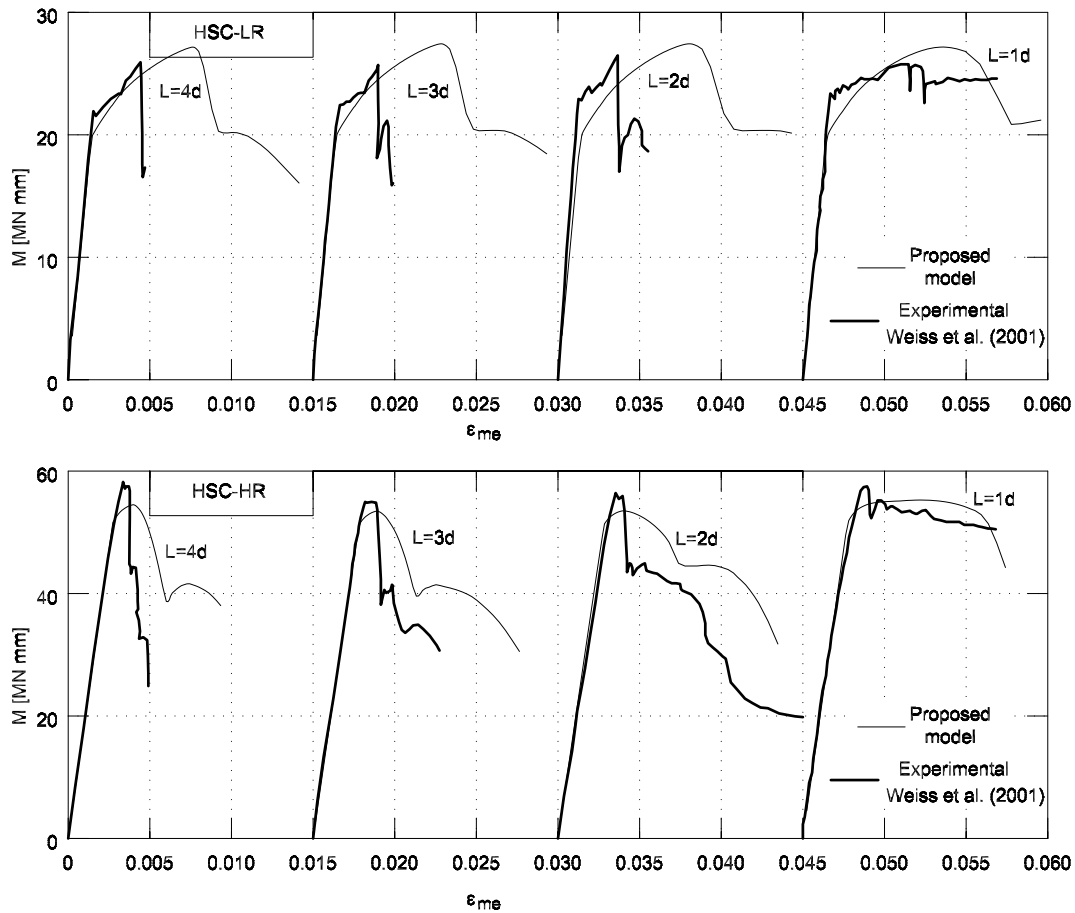


Figure 11. Average compressive top fiber strain  $\epsilon_{me}$  in the constant-moment zone  $L$ : comparison between the numerical results of the proposed model and the experimental ones by Weiss et al. (2001), measured for the beams of high strength concrete (HSC) with high (HR) and low (LR) reinforcement ratio.

## 5 REFERENCES

- Bazant, Z. P. & Xiang, Y. 1997. Size effect in compression fracture: splitting crack band propagation. *J. Engrg. Mech., ASCE* 123(2): 162-172.
- CEB 1991. CEB-FIP Model Code 1990. *Bulletin d'information* 203-205.
- Fantilli, A. P., Ferretti, D., Iori, I. and Vallini, P. 2002a. A Mechanical Model for the Failure of Compressed Concrete in R/C Beams. *J. Struct. Engrg., ASCE* 128(5): 637-645.
- Fantilli, A. P., Iori, I. and Vallini, P. 2002b. Mechanical Model for the Confined Compressed Concrete of RC Beams. In *1st fib Congress: Concrete Structures in the 21st century, October 13-19 2002, Osaka, Japan*.
- Fujita, Y., Ishimaru, R., Hanai, S. and Suenaga, Y. 1998. Study on internal friction angle and tensile strength of plain concrete. In Mihashi H. and Rokugo K. (eds.) *Proc. Fracture Mechanics of Concrete Structures FRAMCOS 3 Gifu, Japan, 1998*. Freiburg: Aedificatio Publishers.
- Hillerborg, A. 1990. Fracture mechanics concepts applied to moment capacity and rotational capacity of reinforced concrete beams. *Engrg. Fracture Mech.* 35(1/2/3): 233-240.
- Jansen, D. C. & Shah, S. P. 1997. Effect of length on compressive strain softening of concrete. *J. Engrg. Mech., ASCE* 123(1): 25-35.
- Markeset, G. & Hillerborg, A. 1995. Softening of concrete in compression - Localization and size effects. *Cement and Concrete Research* 25(4): 702-708.
- Wang, E. Z. & Shrive, N. G. 1995. Brittle fracture in compression: mechanisms, models and criteria. *Engrg. Fracture Mech.* 52(6): 1107-1126.
- Weiss, W. J., Güler K., and Shah, S. P. 2001. Localization and size-dependent response of reinforced concrete beams. *ACI Struct. J.* 98(5): 686-695.